



OPEN

Preclinical comparative study of [¹⁸F]AIF-PSMA-11 and [¹⁸F]PSMA-1007 in varying PSMA expressing tumors

Sarah Piron¹✉, Jeroen Verhoeven², Jan Courty³, Ken Kersemans³, Benedicte Descamps⁴, Leen Pieters⁵, Anne Vral⁵, Christian Vanhove⁴ & Filip De Vos¹

A wide variety of ¹⁸F-labeled PSMA-targeting PET radiotracers have been developed, including [¹⁸F]AIF-PSMA-11. As there is only limited data on the comparison with other ¹⁸F-labeled PSMA PET tracers, a comparative preclinical study between [¹⁸F]AIF-PSMA-11 and [¹⁸F]PSMA-1007 was conducted. Mice with varying PSMA expressing tumors (C4-2, 22Rv1 and PC-3, each n = 5) underwent two PET/CT scans with both [¹⁸F]AIF-PSMA-11 and [¹⁸F]PSMA-1007. Ten additional mice bearing C4-2 xenografts were subjected to ex vivo biodistribution with either [¹⁸F]AIF-PSMA-11 (n = 5) or [¹⁸F]PSMA-1007 (n = 5). Absolute SUV_{mean} and SUV_{max} values were significantly higher for [¹⁸F]PSMA-1007 scans in both C4-2 tumors ($p < 0.01$) and 22Rv1 tumors ($p < 0.01$). In C4-2 xenograft bearing mice, the tumor-to-organ ratios did not significantly differ between [¹⁸F]AIF-PSMA-11 and [¹⁸F]PSMA-1007 for liver, muscle, blood and salivary glands ($p > 0.05$). However, in 22Rv1 xenograft bearing mice, all tumor-to-organ ratios were higher for [¹⁸F]AIF-PSMA-11 ($p < 0.01$). In healthy organs, [¹⁸F]PSMA-1007 uptake was higher in the liver, gallbladder, small intestines and glands. Biodistribution data confirmed the increased uptake in the heart, small intestines and liver with [¹⁸F]PSMA-1007. Absolute tumor uptake was higher with [¹⁸F]PSMA-1007 in all tumors. Tumor-to-organ ratios did not differ significantly in high PSMA expressing tumors, but were higher for [¹⁸F]AIF-PSMA-11 in low PSMA expressing tumors. Furthermore, [¹⁸F]PSMA-1007 showed higher uptake in healthy organs.

Abbreviations

CT	Computed tomography
IHC	Immunohistochemistry
OSEM	Ordered subsets maximization expectation
p.i.	Post injection
PET	Positron emission tomography
PSMA	Prostate specific membrane antigen
SUV	Standardized uptake value
TBR	Tumor-to-blood ratio
TLR	Tumor-to-liver ratio
TMR	Tumor-to-muscle ratio
TSGR	Tumor-to-salivary gland ratio
VOI	Volume of interest

The prostate specific membrane antigen (PSMA) is a type II transmembrane protein that is upregulated on prostate cancer cells¹. Further research showed PSMA to be an excellent target for molecular imaging of prostate carcinoma, which has led to a steep increase in the development of PSMA targeting tracers. Initially, PSMA monoclonal antibodies were introduced targeting either the intracellular domain (7E11 or Capromab Pendetide)

¹Laboratory for Radiopharmacy, Ghent University, Ghent, Belgium. ²Department of Diagnostic Sciences, Ghent University, Ghent, Belgium. ³Department of Medical Imaging, Ghent University Hospital, Ghent, Belgium. ⁴IBiTech-MEDISIP, Department of Electronics and Information Systems, Ghent University, Ghent, Belgium. ⁵Department of Human Structure and Repair, Ghent University, Ghent, Belgium. ✉email: sarah.piron@ugent.be

or extracellular domain (J591) of PSMA^{2,3}. However, monoclonal antibodies have several disadvantageous characteristics for diagnostic purposes, such as a slow tumor uptake and a long circulating half-life. Consequently, the focus of PSMA radiopharmaceutical development has shifted to the development of low molecular weight molecules. These PSMA inhibitors consist usually of a hydrophilic glutamate-urea based pharmacophore coupled to a lipophilic chelator, which target the extracellular zinc pocket and lipophilic pocket of the PSMA protein, respectively. The different affinity of these radiotracers for the PSMA target is determined by the variable amino acid linked to the Glu-urea group and the chelator. Finally, the PSMA inhibitors can be internalized into the cell via clathrin-coated pits^{4,5}. [⁶⁸Ga]PSMA-11 was the first PSMA PET tracer that was widely applied for prostate cancer positron emission tomography/computed tomography (PET/CT) imaging. This PET tracer has demonstrated excellent overall performance in both initial staging (sensitivity of 0.74 (95% CI 0.51–0.89)) and specificity of 0.96 (95% CI 0.85–0.99)) and recurrent prostate cancer (PCa) (detection rate of 0.63 (95% CI, 0.55–0.70) for PSA ≤ 2.0 ng/mL and 0.94 (95% CI, 0.91–0.96) for PSA > 2.0 ng/mL)^{6–9}. However, the cyclotron produced fluorine-18 has superior imaging characteristics, including a longer half-life (110 min vs 68 min), a lower positron energy (0.65 MeV vs 1.90 MeV) and a higher positron yield (97% vs 89%)¹⁰. Therefore, interest in ¹⁸F-labeled PSMA radiopharmaceuticals increased¹¹. As a result, a wide variety of [¹⁸F]PSMA PET tracers were developed, each with its characteristic advantages and disadvantages in terms of availability, ease of synthesis, binding affinity, pitfalls and biodistribution patterns^{12,13}. Out of the extensive pool of [¹⁸F]PSMA PET tracers, [¹⁸F]DCFPyL and [¹⁸F]PSMA-1007 are the most commonly used and their performance has been compared to [⁶⁸Ga]PSMA-11. Studies suggested the non-inferiority of [¹⁸F]DCFPyL compared to [⁶⁸Ga]PSMA-11^{14,15}, as well as a similar biodistribution pattern¹⁶. A comparative pilot study between [¹⁸F]PSMA-1007 and [⁶⁸Ga]PSMA-11 showed that both tracers identified all dominant prostatic lesions, while [¹⁸F]PSMA-1007 detected some additional low-grade lesions¹⁷. A meta-analysis by Liu et al. reported a pooled sensitivity and specificity of 0.923 and 0.442 for PSA > 2 ng/mL and 0.832 and 0.277 for PSA ≤ 2 ng/mL, respectively¹⁸. These results were confirmed by an intra-individual comparative study by Hoberück et al.¹⁹. The authors reported the exchangeability of both tracers depending on the availability, but highlighted the increased incidence of non-specific bone findings with [¹⁸F]PSMA-1007. This finding corresponds to the results of a matched-pair comparison by Rauscher et al. which observed a considerably higher number of benign uptake foci with [¹⁸F]PSMA-1007 (ganglia, 43%; unspecific lymph nodes, 31%; and bone lesions, 24%) compared to [⁶⁸Ga]PSMA-11²⁰.

Based on the binding motif of [⁶⁸Ga]PSMA-11, [¹⁸F]AlF-PSMA-11 was developed. The evaluation in several clinical trials revealed a low radiation burden²¹, good inter-reader reliability²² and non-inferiority with [⁶⁸Ga]PSMA-11²³. However, limited data is available on the comparison of [¹⁸F]AlF-PSMA-11 with other ¹⁸F-PSMA PET tracers such as [¹⁸F]PSMA-1007²⁴. Therefore, the aim of this preclinical study was to compare [¹⁸F]AlF-PSMA-11 to an established ¹⁸F-PSMA PET tracer. For this purpose, [¹⁸F]PSMA-1007 was selected as a comparator because of its widely commercial availability²⁵. This study includes the intra-individual comparison of mice bearing PCa xenografts with varying PSMA expression as well as an ex vivo biodistribution with [¹⁸F]AlF-PSMA-11 and [¹⁸F]PSMA-1007.

Materials and methods

Synthesis of PSMA PET tracers. [¹⁸F]AlF-PSMA-11 was synthesized on a modified SynthraFCHOL synthesis module (Synthra GmbH, Hamburg, Germany) as previously reported²⁶. [¹⁸F]PSMA-1007 was synthesized on an IBA Synthra + platform (IBA, Louvain-la-Neuve, Belgium) as described by Kramer et al.²⁷ using a commercially available kit (ABX, Radeberg, Germany).

Quality control. The radiochemical purity was determined by thin layer chromatography (Alugram RP18-W/UV254 plates (Machery Nagel, Düren, Germany)) using 3:1 v/v acetonitrile in water as mobile phase and resulted in > 96% for [¹⁸F]AlF-PSMA-11 and > 95% for [¹⁸F]PSMA-1007. The molar activity (MA) was determined by high performance liquid chromatography (Prevail C18 reversed-phase column, 4.6 × 250 mm, 5 μm, Lokeren, Belgium) and a calibrated dose calibrator, and resulted in a median activity of 187.0 MBq/nmol (range 181.7 – 190.8 MBq/nmol) for [¹⁸F]AlF-PSMA-11 and 98.2 (range 83.6 – 312.7 MBq/nmol) for [¹⁸F]PSMA-1007 at the end-of-synthesis.

Preparation of tumor models. Prostate cancer cells with varying PSMA expression levels were selected: C4-2 (ATCC® CRL-3314, high PSMA expression), 22Rv1 (ATCC® CRL-2505, low PSMA expression) and PC-3 (ATCC® CRL-1435, no PSMA expression). Cells were cultured using RPMI 1640 medium containing 10% FBS, 1% glutamine 200 mM and 1% penicillin/streptomycin (10,000 U/mL) and maintained at 37 °C in 5% CO₂ in humidified air.

To prepare the cell suspension, the prostate cancer cells were detached, rinsed with FBS-free RPMI 1640 medium and diluted to 5 × 10⁶ cells/100 μL. Four-to-six-week-old male NOD/SCID mice (Janvier, France) were subcutaneously injected at shoulder height with 200 μL 1:1 cell suspension:Matrigel® on either side of each mouse (C4-2, n = 5; 22Rv1, n = 5; PC-3, n = 5). Mice were weekly monitored for tumor growth for 5–6 weeks until tumors reached a diameter between 5 and 10 mm. The study was approved by the Ghent University Ethical Committee on animal experiments (ECD 21/63). All animals were kept and handled according to the European guidelines (Directive 2010/63/EU).

Small animal PET/CT imaging. All mice received two PET/CT scans with both [¹⁸F]AlF-PSMA-11 and [¹⁸F]PSMA-1007 within a timeframe of 4 days (range 1–4 days). All mice were intravenously administered 9.09 ± 0.55 MBq [¹⁸F]AlF-PSMA-11 with a MA of 61.64 ± 15.83 MBq/nmol and 9.72 ± 0.67 MBq [¹⁸F]PSMA-

1007 with a MA of 53.40 ± 16.44 MBq/nmol. One hour after tracer injection, static total-body PET/CT scans were performed for 15 min, followed by a CT scan for co-registration.

The PET images were acquired in list mode using a small animal PET scanner (β -cube, Molecubes, Ghent, Belgium) with a spatial resolution of 0.85 mm and an axial field-of-view of 13 cm. All PET scans were reconstructed into a $192 \times 192 \times 384$ matrix by an ordered subsets maximization expectation (OSEM) algorithm using 30 iterations and a voxel size of $400 \times 400 \times 400$ μ m. High-resolution CT images were acquired using a small animal CT scanner (X-cube, Molecubes, Ghent, Belgium) and iteratively reconstructed with 200 μ m voxel size.

Biodistribution. Ten four-to-six-week-old male NOD/SCID mice (Janvier, France) bearing C4-2 xenografts were subjected to ex vivo biodistribution. All mice received either 2.42 ± 0.09 MBq [^{18}F]AIF-PSMA-11 with a MA of 59.78 ± 11.61 MBq/nmol ($n = 5$) or 2.12 ± 0.11 MBq [^{18}F]PSMA-1007 with a MA of 57.44 ± 12.31 MBq/nmol ($n = 5$). All mice were sacrificed at 1 h post injection (p.i.) and organs including the spleen, intestines, stomach, kidney, bladder, muscle, bone, liver, heart, lungs, brain and testes were removed and collected, as well as a blood sample. All tissues were weighted and measured using a gamma counter (Cobra, Packard, USA).

Immunohistochemical evaluation. After the last scan, two mice/cell line xenografts were sacrificed and tumors were collected for immunohistochemical (IHC) evaluation of the PSMA expression levels as previously reported²⁸. In short, sections were taken from the center of the tumor sample and stained using Haematoxylin/Eosin, incubated with a primary PSMA antibody (1:400, 2 h, ab133579, Abcam) and counterstained using Haematoxylin (Mayer). Sections were digitally scanned with a virtual scanning microscope (Olympus BX51, Olympus Belgium SA/NV, Berchem, Belgium) at high resolution (20 \times magnification).

Data analysis. Co-registration and analysis of the PET/CT images were performed using PMOD (PMOD Technologies[®], Zürich, Switzerland). Volumes of interest (VOIs) were drawn manually for delineating the tumor, kidneys, bladder, salivary, lacrimal and submandibular glands, heart (blood pool), liver, gallbladder, ileum, muscle and bone. Tracer uptake in each VOI was corrected for radioactive decay and residual activity in the syringe. Values were expressed as SUV_{mean} and SUV_{max} . Furthermore, tumor-to-organ ratios including tumor-to-liver (TLR), tumor-to-muscle (TMR), tumor-to-blood (TBR) and tumor-to-salivary gland ratio (TSGR) were determined.

Uptake parameters (SUV_{mean} , SUV_{max} , TLR, TMR, TBR and TSGR) were reported as mean \pm SD. The statistical analysis was performed in R²⁹ using the Wilcoxon-signed ranks test for the cross-over intra-individual comparison of radiotracer uptake per cell line xenograft. The biodistribution results were compared using the Mann–Whitney U test. The significance level was set to $p \leq 0.05$.

Ethics approval and consent to participate. The study was approved by the Ghent University Ethical Committee on animal experiments (ECD 21/63). All animals were kept and handled according to the European guidelines (Directive 2010/63/EU). All methods were carried out in accordance with relevant guidelines and regulations. The study was carried out in compliance with the ARRIVE guidelines.

Results

Comparison of [^{18}F]AIF-PSMA-11 and [^{18}F]PSMA-1007 uptake in varying PSMA expressing xenografts. Mice were inoculated with either a high PSMA expressing cell line (C4-2), a low PSMA expressing cell line (22Rv1) or a PSMA negative cell line (PC-3). Immunohistochemical staining was applied on tumor tissues after the last scan and confirmed the differences in PSMA expression levels (Fig. 1).

Each mouse underwent a static [^{18}F]AIF-PSMA-11 and [^{18}F]PSMA-1007 PET scan for 15 min after an uptake period of 1 h within a median time window of 4 days (range 1–4 days). Representative images of one mouse/cell line xenograft are presented in Fig. 2.

C4-2 tumors (high PSMA expression) and 22Rv1 tumors (low PSMA expression) were clearly visible with both PSMA tracers, but uptake in the latter was less intense. No activity uptake was observed in PC-3 tumors. With both ^{18}F -PSMA tracers, activity uptake was observed in healthy organs including salivary and lacrimal glands, kidneys and bladder. For [^{18}F]PSMA-1007, additional activity uptake was observed in the submandibular glands, intestines and gallbladder. The activity uptake in the glands seems to increase from high PSMA expression (C4-2) to no PSMA expression PC-3).

Absolute SUV_{mean} and SUV_{max} values in both C4-2 tumors (high PSMA expression) and 22Rv1 tumors (low PSMA expression) were significantly higher for [^{18}F]PSMA-1007 scans ($p < 0.01$) (Table 1). In PC-3 tumors (no PSMA expression), the activity uptake was similar between both PSMA PET tracers. In C4-2 xenograft bearing mice, the tumor-to-organ ratios did not significantly differ between [^{18}F]AIF-PSMA-11 and [^{18}F]PSMA-1007 for ratios including TLR_{mean} (liver) (12.68 ± 3.06 vs 14.76 ± 5.82 respectively, $p = 0.2$), TMR_{mean} (muscle) (24.07 ± 4.14 vs 22.22 ± 5.24 , respectively, $p = 0.91$), TBR_{mean} (blood) (12.96 ± 2.61 vs 13.20 ± 2.75 , respectively, $p = 0.73$) and $\text{TSGR}_{\text{mean}}$ (salivary glands) (3.68 ± 1.05 vs 3.58 ± 1.08 , respectively, $p = 0.65$) (Fig. 3). Similar trends were found for maximum tumor-to-organ ratios (Supplementary Data Figure S1). However, in 22Rv1 xenograft bearing mice, all tumor-to-organ ratios were higher for [^{18}F]AIF-PSMA-11, including TLR_{mean} (liver) (5.70 ± 1.46 vs 3.45 ± 0.79 respectively, $p = 0.002$), TMR_{mean} (muscle) (11.68 ± 5.06 vs 5.92 ± 1.58 , respectively, $p = 0.002$), TBR_{mean} (blood) (7.19 ± 1.47 vs 3.72 ± 0.76 , respectively, $p = 0.002$) and $\text{TSGR}_{\text{mean}}$ (salivary glands) (1.48 ± 0.39 vs 0.78 ± 0.18 , respectively, $p = 0.002$). Similar trends were found for maximum tumor-to-organ ratios (Supplementary Data Figure S2).

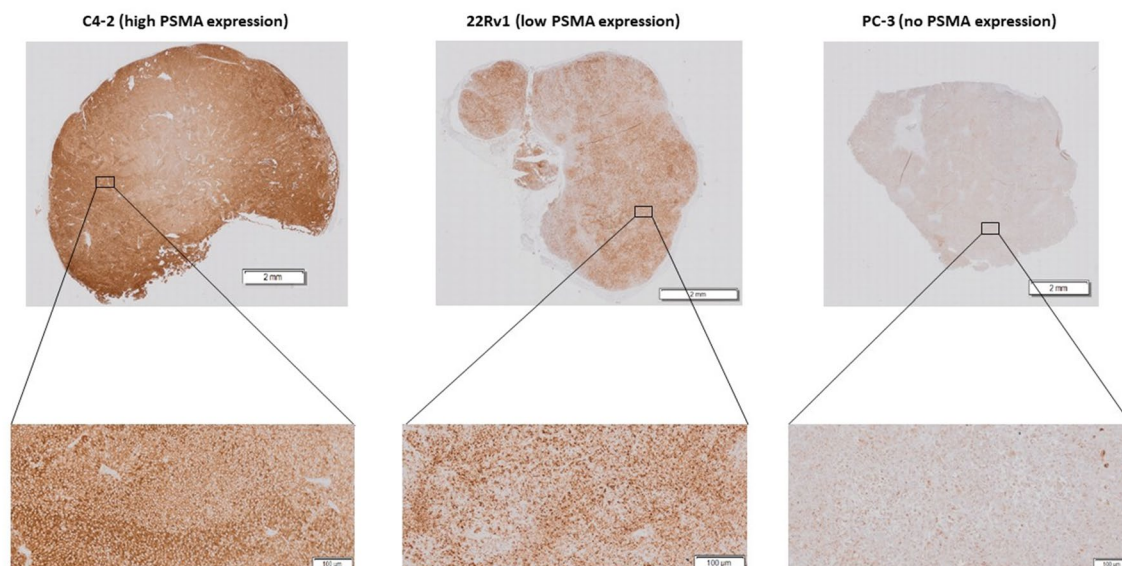


Figure 1. Immunohistochemical staining of tumor tissues of C4-2, 22Rv1 and PC-3 confirming the differences in PSMA expression.

Comparison of [^{18}F]AIF-PSMA-11 and [^{18}F]PSMA-1007 uptake in healthy organs. Comparison of SUV_{mean} values in organs suggests an overall higher activity uptake of [^{18}F]PSMA-1007 in background tissues (Fig. 4). Overall, [^{18}F]AIF-PSMA-11 showed a higher degree of urinary clearance because of higher uptake in the bladder. However, the variability of the uptake values is high because of urination of the mice after injection and before the scan. Compared to [^{18}F]AIF-PSMA-11, a higher amount of [^{18}F]PSMA-1007 was detected in the gallbladder (SUV_{mean} of 0.97 ± 0.51 vs 0.19 ± 0.06 respectively, $p < 0.0001$) and the liver (SUV_{mean} of 0.22 ± 0.07 vs 0.15 ± 0.07 respectively, $p < 0.01$), although the absolute uptake in the liver was relatively low for both PSMA tracers. No statistically significant difference could be observed in the kidneys. All glands (salivary, lacrimal and submandibular) demonstrated higher [^{18}F]PSMA-1007 activity uptake compared to [^{18}F]AIF-PSMA-11, as well as the activity in the heart (blood pool) (SUV_{mean} 0.24 ± 0.06 vs 0.14 ± 0.07 respectively, $p < 0.001$). Increased uptake of [^{18}F]PSMA-1007 was also observed in the intestines with mean SUV_{max} values of 1.40 ± 0.89 with a maximum SUV_{max} value up to 3.33. Finally, no statistically significant difference could be observed in bone (spine) for [^{18}F]PSMA-1007 and [^{18}F]AIF-PSMA-11 (SUV_{mean} 0.44 ± 0.11 vs 0.45 ± 0.11 respectively, $p = 0.46$).

Ex vivo comparison of [^{18}F]AIF-PSMA-11 and [^{18}F]PSMA-1007 uptake in healthy organs. The tracer uptake in healthy organs was more thoroughly investigated by ex vivo biodistribution. Values are presented as percentage injected dose normalized for the weight of the organs (Table 2). Biodistribution data confirmed the increased uptake in the heart, small intestines and liver with [^{18}F]PSMA-1007. Although the uptake in the brain is statistically significant, the absolute values are insignificantly small. Furthermore, no significant difference could be found in the bladder, blood, bone (sternum), large intestines, lungs, spleen, stomach and testes.

Discussion

Currently, there are several PSMA targeting PET tracers used in clinical practice. Several comparative studies between PSMA PET tracers have been conducted^{15,17,20,30–34}. Although most comparative studies have suggested the overall comparable performance of these PET tracers, there are other factors to consider. [^{18}F]PSMA-1007 has a more complex synthesis route including a critical [^{18}F]fluoride azeotropic drying step whereas the synthesis of [^{18}F]AIF-PSMA-11 can be performed in aqueous conditions. Where the PSMA-11 precursor is widely available for purchasing and in-house implementation, [^{18}F]PSMA-1007 is commercially available as cassettes²⁵. Several preclinical comparative studies between [^{18}F]AIF-PSMA-11 and [^{68}Ga]PSMA-11 have been conducted^{35,36}, but data on the comparison with other ^{18}F -labeled PSMA PET tracers is rather limited.

PET images of both C4-2 and 22Rv1 xenograft bearing mice showed higher absolute uptake values for [^{18}F]PSMA-1007 compared to [^{18}F]AIF-PSMA-11, although the difference for the low PSMA expression 22Rv1 tumors is less pronounced. The reported uptake values of [^{18}F]PSMA-1007 for C4-2 tumors (comparable PSMA expression compared to LNCaP³⁷) seem to be in line with previously reported values by Soeda et al. for LNCaP tumors (SUV_{mean} of 1.81 ± 0.57 and SUV_{max} of 5.4 ± 2.6 versus SUV_{mean} of 2.59 ± 0.37 versus SUV_{max} of 5.5 ± 1.0 in this study³⁸).

Although the absolute uptake values were higher for [^{18}F]PSMA-1007, the tumor-to-organ ratios show no significant difference between both tracers in C4-2 tumors (high PSMA expression). Furthermore, the tumor-to-organ ratios for [^{18}F]AIF-PSMA-11 were significantly higher in 22Rv1 tumors (low PSMA expression). This could be explained by the higher uptake of [^{18}F]PSMA-1007 in healthy tissues such as the liver, heart, and glands as well as the less pronounced absolute difference in tumor uptake between both PSMA tracers in low PSMA expressing tumors. These results suggest that [^{18}F]AIF-PSMA-11 can be useful for the detection of lesions in proximity to

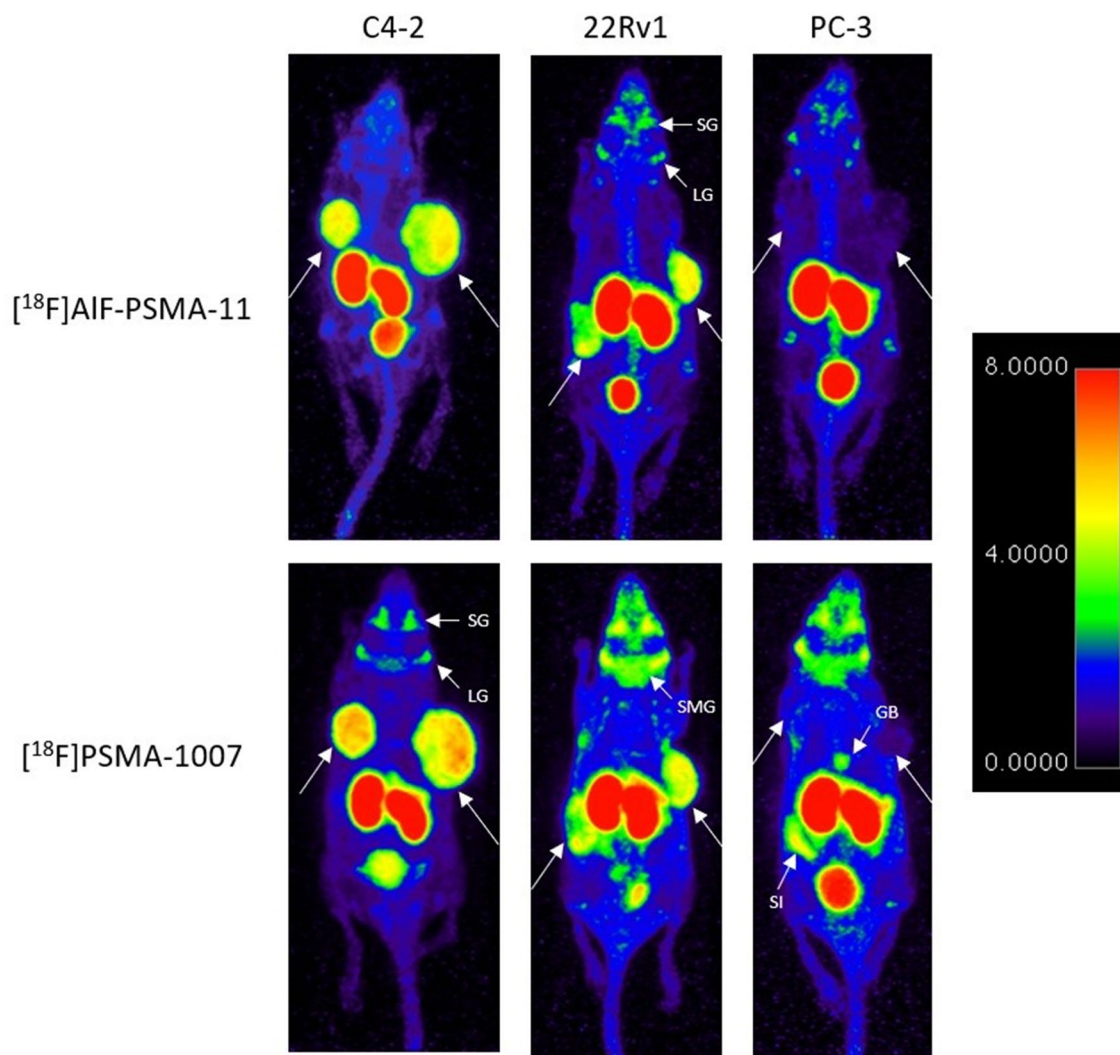


Figure 2. Representative images of mice with either C4-2 (high PSMA expression), 22Rv1 (medium PSMA expression) and PC-3 (no PSMA expression) xenografts. All mice underwent PET/CT imaging 60 min after the administration of [^{18}F]AIF-PSMA-11 and [^{18}F]PSMA-1007. SG = salivary gland, LG = lacrimal gland, SMG = submandibular gland, GB = gallbladder, SI = small intestines. Color maps were generated using Horos v4.0.0, <https://horosproject.org/>.

	SUV _{mean}			SUV _{max}		
	[^{18}F]AIF-PSMA-11	[^{18}F]PSMA-1007	<i>p</i>	[^{18}F]AIF-PSMA-11	[^{18}F]PSMA-1007	<i>p</i>
C4-2	1.65 ± 0.33	2.59 ± 0.37	0.0039	3.58 ± 1.00	5.52 ± 1.00	0.0039
22Rv1	0.64 ± 0.23	0.88 ± 0.21	0.002	1.58 ± 0.59	2.35 ± 0.80	0.0059
PC-3	0.24 ± 0.08	0.22 ± 0.05	0.38	0.50 ± 0.15	0.61 ± 0.20	0.31

Table 1. SUV_{mean} and SUV_{max} values for [^{18}F]AIF-PSMA-11 and [^{18}F]PSMA-1007 uptake in C4-2 (high PSMA expression), 22Rv1 (low PSMA expression) and PC-3 (no PSMA expression). Values are expressed as mean ± SD. SUV = Standardized Uptake Value. Significant values are in bold.

organs with higher [^{18}F]PSMA-1007 uptake such as the gallbladder, liver, heart (blood pool) and small intestines. However, the reverse also applies for the bladder and kidneys, as [^{18}F]AIF-PSMA-11 is primarily renally excreted. Prostate cancer tumors with a low PSMA expression have been shown to be a negative prognostic factor for overall survival. A study by Seifert et al. investigated the correlation between PSMA expression and overall survival in patients who underwent [^{177}Lu]PSMA therapy. Patients with low PSMA expressing lesions were reported to have a shorter survival (7.9 months) compared to patients without low PSMA expressing lesions (21.3 months,

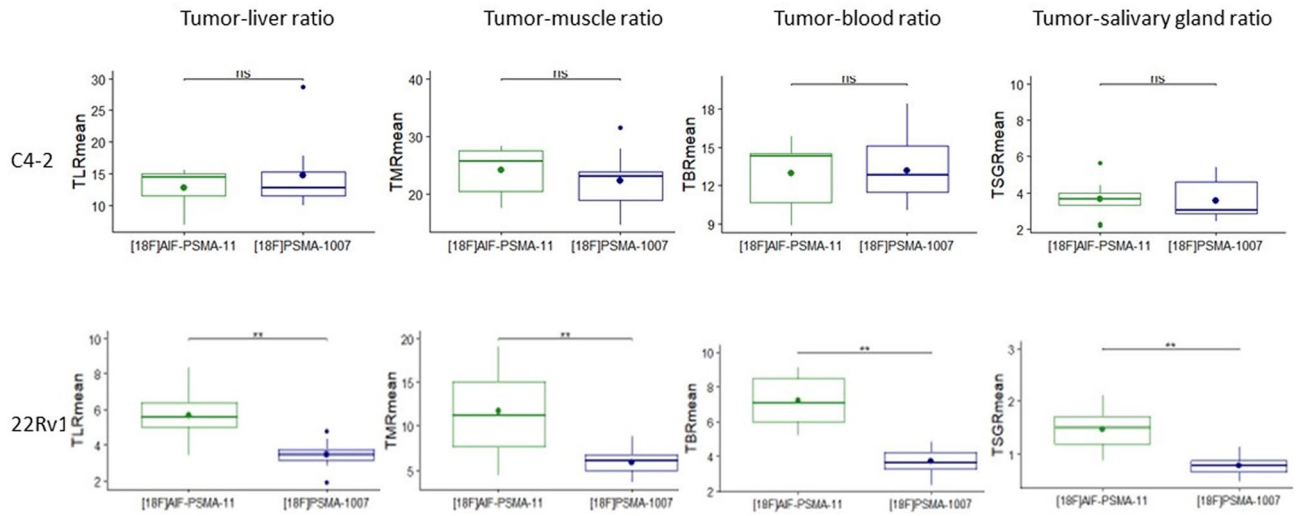


Figure 3. TLR_{mean} (liver), TMR_{mean} (muscle), TBR_{mean} (blood) and TSGR_{mean} (salivary gland) for $[^{18}\text{F}]\text{AIF-PSMA-11}$ and $[^{18}\text{F}]\text{PSMA-1007}$ uptake in C4-2 and 22Rv1 xenograft bearing mice. The dot presents the mean, the horizontal bar presents the median value. Ns= not significant, * = p < 0.05, ** = p < 0.01.

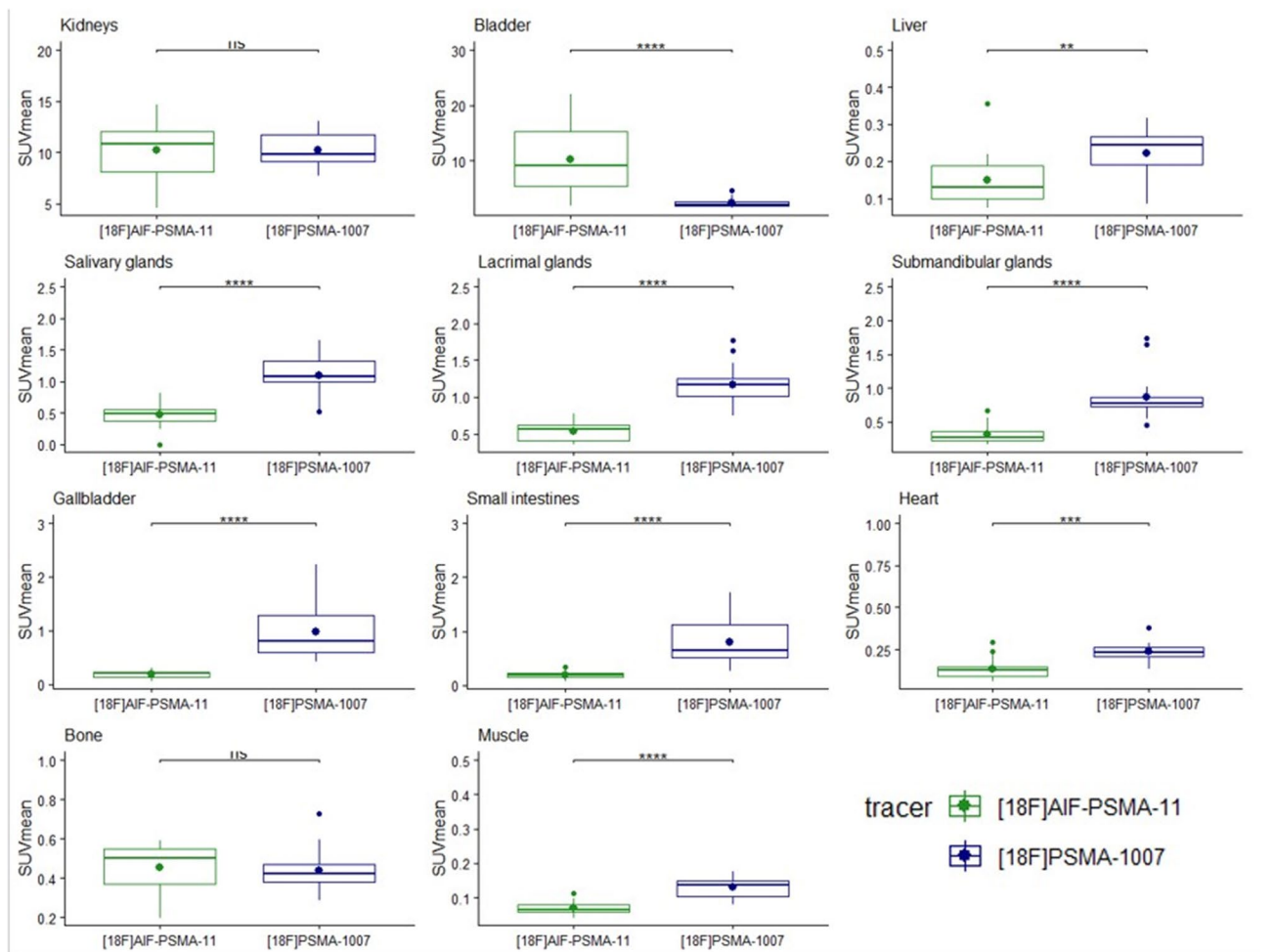


Figure 4. SUV_{mean} for $[^{18}\text{F}]\text{AIF-PSMA-11}$ and $[^{18}\text{F}]\text{PSMA-1007}$ uptake in healthy organs: kidneys, bladder, liver, salivary glands, lacrimal glands, submandibular glands, gallbladder, small intestines, heart and bone. The dot presents the mean, the horizontal bar presents the median value. Ns= not significant, * = p < 0.05, ** = p < 0.01, *** = p < 0.001, **** = p < 0.0001.

Organ	%ID/g		
	[¹⁸ F]AIF-PSMA-11	[¹⁸ F]PSMA-1007	<i>p</i>
Bladder	2.41 ± 0.90	3.13 ± 1.39	0.42
Blood*	0.57 ± 0.15	1.00 ± 0.06	0.016
Bone	1.16 ± 0.34	0.89 ± 0.05	0.42
Brain*	0.05 ± 0.01	0.10 ± 0.02	0.016
Heart*	0.64 ± 0.18	1.33 ± 0.29	0.016
Kidneys**	111 ± 30.10	47.7 ± 12.2	0.0079
Large intestines	0.28 ± 0.13	0.36 ± 0.18	0.55
Small intestines*	0.26 ± 0.08	0.94 ± 0.43	0.016
Liver**	0.39 ± 0.09	1.08 ± 0.38	0.0079
Lungs	1.69 ± 0.31	1.88 ± 0.63	0.84
Spleen	15.28 ± 4.27	18.20 ± 9.2	0.9
Stomach	0.37 ± 0.07	0.46 ± 0.18	0.15
Testes	0.79 ± 0.19	0.68 ± 0.12	0.31

Table 2. Biodistribution data of [¹⁸F]AIF-PSMA-11 and [¹⁸F]PSMA-1007 of healthy organs. The values represent the percentage injected dose per gram tissue weight 1 h after injection. %ID/g = percentage injected dose per gram.

$p = 0.003$). Whether this can be attributed to reduced efficacy of [¹⁷⁷Lu]PSMA therapy or to dedifferentiated and more aggressive tumor phenotypes, remains unclear³⁹. Nevertheless, it remains important to detect the presence of low PSMA expressing metastases to aid in the prognostication and decision making process regarding treatment plan. The higher tumor-to-organ ratios for [¹⁸F]AIF-PSMA-11 compared to [¹⁸F]PSMA-1007 may therefore be beneficial for the detection of low PSMA expressing tumors. This will mostly depend on the location of the lesion, as the absolute tumor uptake remains higher with [¹⁸F]PSMA-1007. Furthermore, the detection of non-prostatic tumors is a potential application these are mostly characterized by a low PSMA expression⁴⁰.

Although the tumor-to-muscle ratio seems to be significantly higher for [¹⁸F]AIF-PSMA-11, the absolute uptake values in the muscle are relatively low (0.13 ± 0.03 for [¹⁸F]PSMA-1007 compared to 0.07 ± 0.02 for [¹⁸F]AIF-PSMA-11), which renders this parameter clinically less relevant. Images in Fig. 2 showed higher activity uptake in glands of mice with PSMA negative tumors compared to high PSMA expressing tumors. This could be attributed to more PSMA binding to the tumor, reducing the amount of PSMA tracer left to bind aspecifically.

As the molar activity has a large influence on the tumor uptake, both radiotracers were administered in comparable MA values (61.6 ± 15.8 MBq/nmol for [¹⁸F]AIF-PSMA-11 and 53.4 ± 16.4 MBq/nmol for [¹⁸F]PSMA-1007). Although [¹⁸F]PSMA-1007 has been reported to achieve molar activities up to 1000 MBq/nmol^{27,38,41}, the study by Soeda et al. showed no significant difference in tumor uptake values between 1000 and 100 MBq/nmol. However, at these higher MA, the uptake in the salivary glands increased significantly³⁸.

Potential defluorination leading to benign bone uptake is always one of the major key points when considering the use of [¹⁸F]AIF-PSMA-11. Although some studies have reported increased bone uptake with [¹⁸F]AIF-PSMA-11^{24,35}, we did not observe this in our study, both in the imaging and biodistribution experiments. This can possibly be explained by the applied storage conditions. As [¹⁸F]AIF-PSMA-11 is less stable at room temperature, the activity vial was cooled until administration of the tracer. The same procedure is maintained when used in our clinical routine and this seems to significantly reduce the defluorination process.

Several organs were difficult to delineate on PET images. For example, the spleen is located too closely to the kidneys to be accurately delineated, and it is difficult to distinguish between the large and small intestine on imaging. Therefore, additional biodistribution data of healthy organs was collected. Although PET images demonstrated increased uptake in the bladder of [¹⁸F]AIF-PSMA-11, biodistribution data did not show a significant difference. This can be explained as the bladder was emptied in the biodistribution experiment while mice were imaged with a full bladder. Therefore, the data suggests that the increased uptake is due to the primarily urinary excretion of [¹⁸F]AIF-PSMA-11. PET images showed increased uptake spots in the intestines with [¹⁸F]PSMA-1007. Biodistribution data revealed a statistically significant higher uptake in the small intestines (0.94 ± 0.43 %ID/g for [¹⁸F]PSMA-1007 vs 0.26 ± 0.08 %ID/g for [¹⁸F]AIF-PSMA-11, $p = 0.016$). These results are consistent with the study by Soeda et al. who also reported increased uptake in the small intestines³⁸. Overall, [¹⁸F]PSMA-1007 seems to accumulate more in healthy organs that express PSMA to a low extent (small intestines, salivary and lacrimal glands, liver and spleen). This might be caused by a higher affinity of [¹⁸F]PSMA-1007 compared to [⁶⁸Ga]PSMA-11^{42,43}, which has been shown to have a similar affinity to [¹⁸F]AIF-PSMA-11³⁶. Although this probably leads to the superior tumor uptake, this also causes more aspecific uptake in non-tumor tissue, increasing the background activity. A matched-pair comparative study evaluating the frequency of benign uptake for [¹⁸F]PSMA-1007 and [⁶⁸Ga]PSMA-11, suggested that five times more lesions (245 out of 369 PSMA-uptake positive lesions) could be attributed to a benign origin for [¹⁸F]PSMA-1007 compared to 52 of 178 PSMA-uptake positive lesions for [⁶⁸Ga]PSMA-11²⁰. This difference was attributed to either the higher affinity of [¹⁸F]PSMA-1007 and the superior spatial resolution of fluorine-18. An overview of the strengths and weaknesses of both radiotracers is given in Table 3.

	¹⁸ F]AIF-PSMA-11	¹⁸ F]PSMA-1007
Strengths	Simple, straightforward synthesis in aqueous conditions	Commercially available cassette system
	Precursor is freely available	Stable at room temperature
	High PSMA affinity leads to specific tumor uptake and low non-tumor uptake in healthy organs	Very high PSMA affinity leads to specific and high absolute tumor uptake
	Low uptake in healthy organs results in high tumor-to-organ ratios	Low urinary clearance causes less interference for the detection of local recurrent disease
Weaknesses	No commercially available synthesis platform	More complex synthesis with azeotropic drying step
	End product should be cooled to ensure the stability over a longer time period	Very high PSMA affinity leads to uptake in non-tumor tissues including salivary, lacrimal and submandibular glands, gall bladder, small intestines and spleen
	Lower absolute tumor uptake	High uptake in background tissues results in lower tumor-to-organ ratios
	Renal clearance leads to high activity in the bladder, which could interfere with the detection of local recurrent disease	Hepatobiliary clearance leads to higher tracer uptake in de liver, potentially obscuring liver lesions

Table 3. Overview of the strengths and weaknesses of [¹⁸F]AIF-PSMA-11 and [¹⁸F]PSMA-1007.

The major limitation to this study is the difference in PSMA expressing tissues between mice and humans. Because of the high PSMA expression in murine kidneys, it is possible that kidney activity in humans may give different results. However, imaging and biodistribution data concerning the bladder and liver suggests that the primary excretion pathway for [¹⁸F]PSMA-1007 (hepatobiliary clearance) and [¹⁸F]AIF-PSMA-11 (urinary clearance) is comparable between mice and humans.

Conclusion

Both [¹⁸F]AIF-PSMA-11 and [¹⁸F]PSMA-1007 demonstrated good image quality. High and low PSMA expressing tumors demonstrated higher absolute tumor uptake with [¹⁸F]PSMA-1007, but tumor-to-organ ratios did not differ significantly and were higher with [¹⁸F]AIF-PSMA-11 in low PSMA expressing xenograft bearing mice. This may be attributed to increased [¹⁸F]PSMA-1007 uptake in healthy organs such as the liver, heart and salivary glands but also in the gallbladder and small intestines. Whether these preclinical observations will result in clinically relevant differences between both radiotracers should be further investigated.

Data availability

The datasets generated during the current study are available from the corresponding author on reasonable request.

Received: 27 July 2022; Accepted: 8 September 2022

Published online: 21 September 2022

References

- Wright, G. L., Haley, C., Beckett, M. L. & Schellhammer, P. F. Expression of prostate-specific membrane antigen in normal, benign, and malignant prostate tissues. *Urol. Oncol.* **1**, 18–28 (1995).
- Taneja, S. S. ProstaScint(R) Scan: Contemporary use in clinical practice. *Rev. Urol.* **6**(Suppl 10), S19-28 (2004).
- Smith-Jones, P. M. *et al.* Radiolabeled monoclonal antibodies specific to the extracellular domain of prostate-specific membrane antigen: Preclinical studies in nude mice bearing LNCaP human prostate tumor. *J. Nucl. Med.* **44**, 610–617 (2003).
- Ghosh, A. & Heston, W. D. W. Tumor target prostate specific membrane antigen (PSMA) and its regulation in prostate cancer. *J. Cell. Biochem.* <https://doi.org/10.1002/jcb.10661> (2004).
- Eiber, M., Fendler, W.P., Rowe, S.P., Calais, J., Hofman, M.S., Maurer, T., *et al.* Prostate-specific membrane antigen ligands for imaging and therapy. *J. Nucl. Med. Society of Nuclear Medicine Inc.*; p. 67S-76S (2017).
- Hirnas, N. *et al.* [68Ga]PSMA PET/CT improves initial staging and management plan of patients with high-risk prostate cancer. *Mol. Imaging Biol.* **21**, 574–81 (2019).
- Perera, M., Papa, N., Christidis, D., Wetherell, D., Hofman, M.S., Murphy, D.G., *et al.* Sensitivity, specificity, and predictors of positive 68Ga-prostate-specific membrane antigen positron emission tomography in advanced prostate cancer: a systematic review and meta-analysis [Internet]. *Eur. Urol. Elsevier*; 2016. pp. 926–37. <https://www.sciencedirect.com/science/article/pii/S0302283816302937>
- Fendler, W. P. *et al.* Assessment of 68Ga-PSMA-11 PET accuracy in localizing recurrent prostate cancer: A prospective single-arm clinical trial. *JAMA Oncol.* **5**, 856–63 (2019).
- Hope, T. A. *et al.* Metaanalysis of 68 Ga-PSMA-11 PET accuracy for the detection of prostate cancer validated by histopathology. *J. Nucl. Med.* **60**, 786–93 (2019).
- Sanchez-Crespo, A. Comparison of Gallium-68 and Fluorine-18 imaging characteristics in positron emission tomography. *Appl. Radiat. Isot.* **76**, 55–62 (2013).
- Kesch, C., Kratochwil, C., Mier, W., Kopka, K., Giesel, F.L. 68Ga or 18F for prostate cancer imaging?. *J. Nucl. Med.* 2017. p. 687–8. <http://jnmm.snmjournals.org/content/early/2017/04/12/jnumed.117.190157.full.pdf>
- Werner, R. A. *et al.* 18 F-Labeled, PSMA-targeted radiotracers: Leveraging the advantages of radiofluorination for prostate cancer molecular imaging. *Theranostics* **10**, 1–16 (2020).
- Piron, S., Verhoeven, J., Vanhove, C., De Vos, F. Recent advancements in 18F-labeled PSMA targeting PET radiopharmaceuticals. *Nucl. Med. Biol. Elsevier*; 2022, p. 29–51. <https://linkinghub.elsevier.com/retrieve/pii/S0969805121005345>
- Dietlein, F. *et al.* PSA-stratified performance of 18F-and 68Ga-PSMA PET in patients with biochemical recurrence of prostate cancer. *J. Nucl. Med.* **58**, 947–52 (2017).
- Dietlein, M. *et al.* Comparison of [18F]DCFPyL and [68Ga]Ga-PSMA-HBED-CC for PSMA-PET imaging in patients with relapsed prostate cancer. *Mol. Imaging Biol.* **17**, 575–84 (2015).

16. Ferreira, G., Iravani, A., Hofman, M. S. & Hicks, R. J. Intra-individual comparison of 68Ga-PSMA-11 and 18F-DCFPyL normal-organ biodistribution. *Cancer Imaging* **19**, 1–10 (2019).
17. Kuten, J. *et al.* Head-to-head comparison of 68Ga-PSMA-11 with 18F-PSMA-1007 PET/CT in staging prostate cancer using histopathology and immunohistochemical analysis as a reference standard. *J. Nucl. Med.* **61**, 527–32 (2020).
18. Liu, X., Wang, Q., Zhang, B., Jiang, T. & Zeng, W. Diagnostic accuracy of 18F-PSMA-1007 PET/CT for prostate cancer in primary staging and biochemical recurrence with different serum PSA levels: A systematic review and meta-analysis. *Hell J. Nucl. Med.* **25**, 88–102 (2022).
19. Hoberück, S. *et al.* Intra individual comparison of [68 Ga]-Ga-PSMA-11 and [18F]-F-PSMA-1007 in prostate cancer patients: a retrospective single-center analysis. *EJNMMI Res.* **11**, 1–18 (2021).
20. Rauscher, I. *et al.* Matched-pair comparison of 68Ga-PSMA-11 PET/CT and 18F-PSMA-1007 PET/CT: Frequency of pitfalls and detection efficacy in biochemical recurrence after radical prostatectomy. *J. Nucl. Med.* **61**, 51–7 (2020).
21. Piron, S. *et al.* Radiation dosimetry and biodistribution of 18F-PSMA-11 for PET imaging of prostate cancer. *J. Nucl. Med.* **60**, 1736–1742 (2019).
22. Piron, S. *et al.* Optimization of PET protocol and interrater reliability of 18F-PSMA-11 imaging of prostate cancer. *EJNMMI Res.* **10**, 14 (2020).
23. De Man, K., Laeken, N., Van, Schelfhout, V., Fendler, W.P., Lambert, B., Kersemans, K., *et al.* 18F-PSMA-11 Versus 68Ga-PSMA-11 positron emission tomography/computed tomography for staging and biochemical recurrence of prostate cancer: a prospective double-blind randomised cross-over trial. *Eur. Urol.* 2022; <http://www.europeanurology.com/article/S0302283822023831/fulltext>
24. Ioppolo, J. A. *et al.* Direct in vivo comparison of [18F]PSMA-1007 with [68Ga]Ga-PSMA-11 and [18F]AlF-PSMA-11 in mice bearing PSMA-expressing xenografts. *Appl. Radiat. Isot.* **161**, 109164 (2020).
25. Cardinale, J. *et al.* Procedures for the GMP-compliant production and quality control of [18F]PSMA-1007: A next generation radiofluorinated tracer for the detection of prostate cancer. *Pharmaceuticals* **10**, 77 (2017).
26. Kersemans, K. *et al.* Automated radiosynthesis of Al[18 F]PSMA-11 for large scale routine use. *Appl. Radiat. Isot.* **135**, 19–27 (2018).
27. Kramer, V., Fernandez, R., Sandoval, M.P., Gameiro, C., Goblet, D., Müller, M., *et al.* Routine production of [18 F]PSMA-1007 and first clinical experience in staging of prostate cancer patients. 2018.
28. Piron, S. *et al.* Impact of the molar activity and PSMA expression level on [18F]AlF-PSMA-11 uptake in prostate cancer. *Sci. Rep.* **11**, 22623 (2021).
29. R Core Team. R: A language and environment for statistical computing. R Foundation for Statistical Computing [Internet]. 2019 [cited 2019 Jun 5]. Available from: <https://www.r-project.org/>
30. Berliner, C. *et al.* Detection rate of PET/CT in patients with biochemical relapse of prostate cancer using [68Ga]PSMA I&T and comparison with published data of [68Ga]PSMA HBED-CC. *Eur. J. Nucl. Med. Mol. Imaging* **44**, 670–7 (2017).
31. Giesel, F. L. *et al.* Intraindividual comparison of 18 F-PSMA-1007 and 18 FDCFPyL PET/CT in the prospective evaluation of patients with newly diagnosed prostate carcinoma: A pilot study. *J. Nucl. Med.* **59**, 1076–80 (2018).
32. Kroenke, M. *et al.* Matched-pair comparison of 68 Ga-PSMA-11 and 18 F-rhPSMA-7 PET/CT in patients with primary and biochemical recurrence of prostate cancer: frequency of non-tumor related uptake and tumor positivity. *J. Nucl. Med.* **120**, 251447 (2020).
33. Dietlein, F. *et al.* Intraindividual comparison of 18F-PSMA-1007 with renally excreted PSMA ligands for PSMA PET imaging in patients with relapsed prostate cancer. *J. Nucl. Med.* **61**, 729–34 (2020).
34. Wondergem, M., van der Zant, F. M., Broos, W. A. & Knol, R. J. Matched-pair comparison of 18 F-DCFPyL PET/CT and 18 F-PSMA-1007 PET/CT in 240 prostate cancer patients; inter-reader agreement and lesion detection rate of suspected lesions. *J. Nucl. Med. [Internet]* **120**, 258574 (2021).
35. Lütje, S. *et al.* In vitro and in vivo characterization of an 18 F-AlF-labeled PSMA ligand for imaging of PSMA-expressing xenografts. *J. Nucl. Med. [Internet]* **60**, 1017–22 (2019).
36. Piron, S. *et al.* Intra-individual dynamic comparison of 18F-PSMA-11 and 68Ga-PSMA-11 in LNCaP xenograft bearing mice. *Sci. Rep.* **10**, 1–11 (2020).
37. Michalska, M. *et al.* In vitro and in vivo effects of a recombinant anti-PSMA immunotoxin in combination with docetaxel against prostate cancer. *Oncotarget.* **7**, 22531–42 (2016).
38. Soeda, F. *et al.* Impact of 18F-PSMA-1007 uptake in prostate cancer using different peptide concentrations: Preclinical PET/CT study on mice. *J. Nucl. Med.* **60**, 1594–9 (2019).
39. Seifert, R. *et al.* Analysis of PSMA expression and outcome in patients with advanced prostate cancer receiving 177Lu-PSMA-617 radioligand therapy. *Theranostics* **10**, 7812–20 (2020).
40. Nimmagadda, S. *et al.* Low-level endogenous PSMA expression in nonprostatic tumor xenografts is sufficient for in vivo tumor targeting and imaging. *J. Nucl. Med.* **59**, 486–93 (2018).
41. Naka, S. *et al.* Automated [18F]PSMA-1007 production by a single use cassette-type synthesizer for clinical examination. *EJNMMI Radiopharm. Chem.* **5**, 1–17 (2020).
42. Eder, M. *et al.* 68Ga-complex lipophilicity and the targeting property of a urea-based PSMA inhibitor for PET imaging. *Bioconjug* **23**, 688–97 (2012).
43. Cardinale, J. *et al.* Preclinical evaluation of 18F-PSMA-1007, a new prostate-specific membrane antigen ligand for prostate cancer imaging. *J. Nucl. Med.* **58**, 425–31 (2017).

Author contributions

The study design was set up by S.P., J.C., K.K. and F.D.V. Data collection and interpretation was carried out by S.P., J.V., B.D., A.V., L.P. and C.V. Image analysis was performed by S.P. J.C. and K.K. were responsible for the production of the investigational products. S.P. drafted the manuscript. All authors read and approved the final manuscript.

Funding

BD was supported by FWO I000321N.

Competing interests

The authors declare no competing interests.

Additional information

Supplementary Information The online version contains supplementary material available at <https://doi.org/10.1038/s41598-022-20060-7>.

Correspondence and requests for materials should be addressed to S.P.

Reprints and permissions information is available at www.nature.com/reprints.

Publisher's note Springer Nature remains neutral with regard to jurisdictional claims in published maps and institutional affiliations.



Open Access This article is licensed under a Creative Commons Attribution 4.0 International License, which permits use, sharing, adaptation, distribution and reproduction in any medium or format, as long as you give appropriate credit to the original author(s) and the source, provide a link to the Creative Commons licence, and indicate if changes were made. The images or other third party material in this article are included in the article's Creative Commons licence, unless indicated otherwise in a credit line to the material. If material is not included in the article's Creative Commons licence and your intended use is not permitted by statutory regulation or exceeds the permitted use, you will need to obtain permission directly from the copyright holder. To view a copy of this licence, visit <http://creativecommons.org/licenses/by/4.0/>.

© The Author(s) 2022